Theory of Gradient Coil Design Methods for Magnetic Resonance Imaging

S.S. HIDALGO-TOBON

Departamento de Ingenieria Electrica, Universidad Autónoma Metropolitana Iztapalapa, Av. San Rafael Atlixco 186, México D.F. 09340, México

ABSTRACT: The process to produce an MR image includes nuclear alignment, RF excitation, spatial encoding, and image formation. In simple terms, an magnetic resonance imaging (MRI) system consists of five major components: a magnet, gradient systems, an RF coil system, a receiver, and a computer system. To form an image, it is necessary to perform spatial localization of the MR signals, which is achieved using gradient coils. In modern MRI, gradient coils able to generate high gradient strengths and slew rates are required to produce high imaging speeds and improved image quality. MRI also requires the use of gradient coils that generate magnetic fields, which vary linearly with position over the imaging volume. Gradient coils for MRI must therefore have high current efficiency (defined as the ratio of gradient generated to current drawn), short switching time (i.e., low inductance), gradient linearity over a large volume, low power consumption, and minimal interaction with any other equipment, which would otherwise result in eddy currents. Over the last two decades new methods of gradient coil design have been developed, and a combination of these methods can be a mixture of them trying to avoid discomforts to patients that at the end is the center of all the technological efforts in the art of MRI. © 2010 Wiley Periodicals, Inc. Concepts Magn Reson Part A 36A: 223–242, 2010.

KEY WORDS: magnetic resonance imaging; gradient coil design; target field method; acoustic noise; review

I. INTRODUCTION

In 1973, Lauterbur and Mansfield (*1*, *2*) independently described the use of nuclear magnetic resonance to form an image. For this work, they shared the Nobel Prize for Medicine in 2003. This imaging modality was named NMR imaging, standing for nuclear magnetic resonance imaging (MRI); however, due to the widespread concern over the word "nuclear," the acronym was soon changed to MRI. This imaging

modality is a powerful tool because of its flexibility and sensitivity to a broad range of tissue properties. Its noninvasive nature makes it a widely used technique for the diagnosis of a variety of diseases. The basic components of the magnetic resonance imaging (MRI) scanner include the main magnet, RF pulse transmitter, RF receiver, gradient coils, data acquisition system, power supplies, and cooling systems. The magnet produces a homogeneous static field along the z direction, which aligns the nuclear spins of hydrogen atoms in the patient and following an RF excitation causes them to precess in perfect concert. The nuclei emit maximum-strength electromagnetic waves immediately after excitation, but over time, the precessing spins get out of synch, often due to small differences in local magnetic fields. The desynchronization of spin precession causes the combined electromagnetic signal to decay with time, a phenomenon called relaxation. A slice is selected applying a gradient in a particular direction (X, Y, or Z) during RF excitation. Magnetic resonance signals are then spatially encoded by means of the application of magnetic field gradients along three different directions. Finally, the signals are acquired and Fourier transformed to form a two-dimensional or three-dimensional image.

II. THEORY

One of the most important concepts for obtaining an image using MRI is the use of magnetic field gradients. How did the gradient become a fundamental part of MRI? In 1973, Mansfield (1) and Lauterbur (2) (Nobel Prize for Medicine and Physiology 2003) proposed the idea of using a "gradient" that spatially encodes the positions of the nuclei of hydrogen within a sample by causing a variation in Larmor frequency as a function of their position. This article describes in detail the characteristics of an ideal field gradient coil and the different methods of designing gradient coils for MRI applications. To understand how a gradient coil works, it is important to understand electromagnetic theory, as basic principles and concepts will help in describing the function of a gradient coil.

Maxwell's Equations

Electromagnetic theory can be described using Maxwell's (3) equations.

$$\nabla \cdot \mathbf{B} = 0 \quad \text{(no magnetic charges)}$$
$$\nabla \cdot \mathbf{D} = \rho \quad \text{(Gauss's law)}$$

$$\nabla \times \mathbf{E} + \frac{\partial \mathbf{B}}{\partial t} = 0 \quad \text{(Faraday's law)}$$
$$\nabla \times \mathbf{H} = \mathbf{J} + \frac{\partial \mathbf{D}}{\partial t} \quad \text{(Ampere's law)} \qquad [1a]$$

where $\mathbf{E}$ and $\mathbf{B}$ are the electric and magnetic fields, and $\mathbf{D}$ and $\mathbf{H}$ have a correspondence with $\mathbf{E}$, and $\mathbf{B}$ through the polarization and the magnetization $\mathbf{M}$ of the material medium by:

$$\mathbf{D} = \varepsilon_0 \mathbf{E} + \mathbf{P} = \varepsilon \mathbf{E} \quad \mathbf{H} = \frac{1}{\mu_0}\mathbf{B} - \mathbf{M} = \frac{\mathbf{B}}{\mu}, \qquad [1b]$$

where ε_0 and μ_0 are the permittivity and permeability of the vacuum, and ε and μ are the permittivity and permeability of the medium. The electric charge density is ρ and the electric current density is $\mathbf{J}$.

A further useful equation is the continuity equation relating charge and current density,

$$\frac{\partial \rho}{\partial t} + \nabla \cdot \mathbf{J} = 0. \qquad [2]$$

The Lorentz force equation describes the force acting on a point charge, q, moving at velocity, $\mathbf{v}$, in the presence of electromagnetic fields.

$$\mathbf{F} = q(\mathbf{E} + \mathbf{v} \times \mathbf{B}). \qquad [3]$$

It is important to mention that in MRI, the static field is by definition time independent, while the magnetic gradient field has mild time dependence usually varying at audio frequencies. In general, magnetic field gradients can therefore be described using quasi-static methods.

The Biot-Savart Law

The Biot-Savart law (1820) allows calculation of the magnetic field generated by the current that circulates through the wires of a gradient coil. This is accomplished by dividing the wires into small elements $I d\mathbf{l}$, flowing in a line element $d\mathbf{l}$ at a distance $\mathbf{r}$ from the point in question (3) (Fig. 1). The Biot-Savart law in its differential form is then:

$$d\mathbf{B} = \frac{\mu_0}{4\pi} I \frac{d\mathbf{l} \times \mathbf{r}}{|\mathbf{r}|^3} \qquad [4]$$

III. REQUIREMENTS FOR GRADIENTS

Three orthogonal gradient coils are required to generate a linear variation of the z-component of the magnetic field along the Cartesian axes x, y, and z:
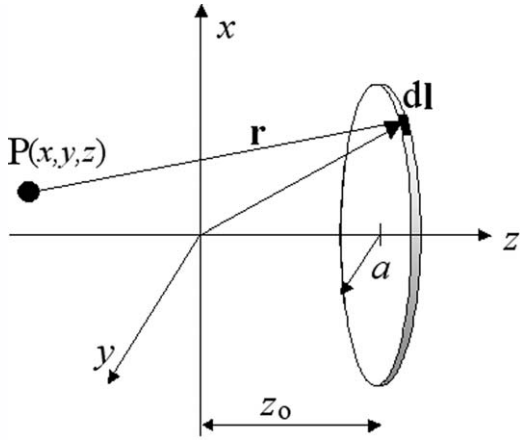
Figure 1 The field at position $P(\mathbf{r})$ due to a wire loop is calculated using the Biot-Savart law.

$$G_x = \frac{\partial B_z}{\partial x} \quad G_y = \frac{\partial B_z}{\partial y} \quad G_z = \frac{\partial B_z}{\partial z}, \qquad [5]$$

where G_x and G_y are referred to as transverse gradients, and G_z is the longitudinal gradient (see Fig. 2). Gradients are produced by passing current, I, through wire coils arranged on a cylindrical surface and gradient strength is measured in T m^{-1} or G cm^{-1}. The gradient strengths used in medical imaging are usually less than 4 G cm^{-1} = 0.04 T m^{-1}. An ideal efficient gradient coil system will produce a given gradient over a large volume for a minimum amount of stored magnetic energy, thus allowing the magnetic field to be switched rapidly. This is achieved only if the gradient coil has low inductance, L. It is also important to keep the coil's resistance, R, as small as possible to reduce power dissipation. Minimal interaction of the gradient coils field with other conducting material is important as this reduces to a minimum the generation of eddy currents (4–9). Achievement of these characteristics generally requires some compromise. For example, increasing the volume over which the gradient is uniform increases the stored magnetic energy and as a consequence, the inductance; rapid gradient switching can also lead to the generation of a large amount of acoustic noise and peripheral nerve stimulation of the patient. The quality of a gradient coil for use in medical imaging depends largely on its inductance, efficiency, and gradient homogeneity.

The gradient homogeneity is related to the difference between the desired field $B_0(\mathbf{r})$ and the field actually achieved over the volume of interest $B(\mathbf{r})$, and can be written as,

$$\frac{1}{V} \int d\mathbf{r} \left(\frac{B(\mathbf{r})}{B_0(\mathbf{r})} - 1 \right)^2 \qquad [6]$$

where V is the volume of integration.

The size of the uniform region of a gradient coil is defined as the diameter of spherical volume (DSV) for consistency with the magnet formula reported by Xu et al. (10). Specifically, the DSV for a gradient coil is defined to be the diameter of the largest sphere within which the gradient field error is not larger than some given percent (e.g., 50%) of the gradient value at the center of the sphere. This error is also called "differential linearity error" to make a clear distinction with the absolute field error, often used by manufacturers in characterizing gradient linear region sizes. The 50% DSV was used to define uniformity region diameter consistently in this study. The choice of the error function can have an important effect on the resulting design and the appearance of an image. For example, if the error is defined as the difference between the actual and desired magnetic field, errors are stressed in spatial position, which are proportional to the field errors, rather than the local distortion of an object, which is proportional to errors in the gradient of the field. Using the error in the magnetic field strongly decreased the homogeneity requirement on points near the central plane of the coil, where the field is near zero. Another reason for minimizing the error in the magnetic gradient field is that diffusion sensitivity is determined by the square of the gradient field. The field error could be measured, ΔB_z, at any point $\mathbf{r}$, using:

$$\Delta B_z(\mathbf{r}) = \frac{\left[B_z(\mathbf{r}) - B_z^{\text{ideal}}(\mathbf{r})\right]}{\max\left(\left|B_z^{\text{Max−ideal}}(\mathbf{r}_{\text{max}})\right|\right)} \cdot 100 \qquad [7]$$
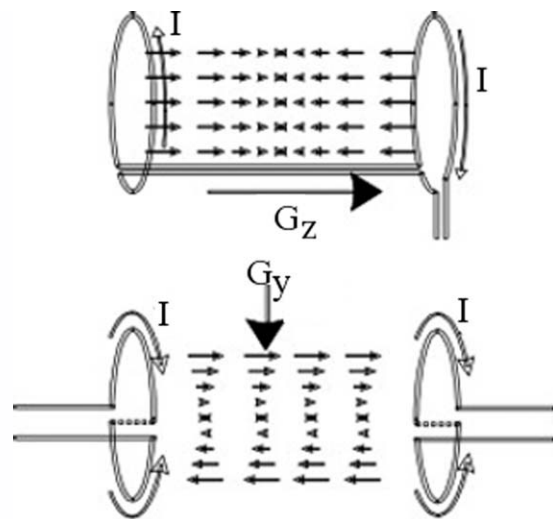

Figure 2 G_z produces a variation of z-component of the magnetic field along the z axis. G_y produces a variation of z-component of the magnetic field along the y axis.

where $B_z(\mathbf{r})$ is the z-component of the magnetic field at $\mathbf{r}$ that the coil generates when 1 amp is passed through it; $B_z^{\text{ideal}}(\mathbf{r})$ is the ideal field and B_z^{Max}-*ideal* ($\mathbf{r}_{\text{max}}$) is the maximum value of $B_z^{\text{ideal}}(\mathbf{r})$ inside the region of uniformity.

The strength of the magnetic field gradient produced by a gradient coil is directly proportional to the current which it carries, so that:

$$G = \eta I \qquad [8]$$

where η is known as the gradient coil efficiency and is usually defined as the field gradient strength at the origin per unit current (T m^{-1} A^{-1}). A gradient coil with a high efficiency will produce a large gradient per unit current. The coil efficiency is mostly influenced by its geometry: the smaller the radius, the more efficient the coil is. Another measure of coil performance has been suggested by Turner (4, 5): this figure of merit is defined as the coil efficiency squared divided by the product of the inductance and the fractional root-mean-square departure from the required field variation in the region of interest (ROI):

$$\beta = \frac{\eta^2/L}{\left[\frac{1}{V}\int d\mathbf{r}\left(\frac{B(\mathbf{r})}{B_0(\mathbf{r})} - 1\right)^2\right]^{\frac{1}{2}}} . \qquad [9]$$

This figure is independent of the number of turns of the coil; it depends only on the configuration and radius of the coil. For the purpose of comparison, the radius of a coil can be scaled to 1.0 m.

The inductance of a gradient coil is an important factor for rapid gradient switching, as a large coil inductance can reduce the switching speed. The resistance must be kept small to limit the power consumption, and another way to reduce the rise time is by adjusting the voltage applied to the gradient coil at the cost of using a more powerful gradient driver. For a gradient coil, the rise time is a function of the inductance (L) and resistance (R) of the coil, the maximum I and the voltage V supplied by the gradient amplifiers (7):

$$\tau = \frac{LI}{V - RI} . \qquad [10]$$

Analysis of the slew rate is another way to evaluate the performance of a gradient coil. Slew rate is given by:

$$S = \frac{G_{\text{max}}}{\tau} = \frac{\eta(V - RI)}{L} . \qquad [11]$$

The inductance plays an important role in limiting the rise time (or the slew rate), so that most approaches to gradient coil design use an inductance minimization constraint as a way to improve performance. In general, the inductance of a cylindrical gradient coil at fixed efficiency is proportional to the fifth power of the coil radius. For this reason, it is important to keep coils as small as possible. It is also important to consider the magnetic energy, W_{S}, stored within the coil which is given by:

$$W_{\text{S}} = \frac{1}{2}LI^2 \qquad [12]$$

this governs the speed with which the field can be switched from one level to another. For a coil with n turns on a cylinder of radius a, the magnetic energy is related to the efficiency factor (8),

$$\frac{G^2}{W_{\text{S}}} = \frac{2G^2}{LI^2} = \frac{2\eta^2}{L} \propto a^{-5} \qquad [13]$$

and the power consumption is related to the resistance by,

$$\frac{G^2}{\text{Power.Consumption}} = \frac{\eta^2}{R} \propto a^{-3} \qquad [14]$$

where it has been assumed that the coil resistance scales as a^{-1}. From Eqs. [13] and [14], it can be seen that it is sensible to design gradient coils as small as possible. The power dissipated by a coil of resistance, R, carrying current, I, is I^2R. Large power dissipation leads to significant heating of the coil wires, potentially leading to coil failure. Although small coils are ideal in performance, the minimum coil size is limited by two constraints: achieving adequate gradient linearity over a volume of interest and allowing straightforward access of the patient to the imaging area. Inductance has become an important factor in the design of gradient coils due to the use of advanced applications of MRI such as functional MRI, diffusion tractography, and perfusion (7, 11).

The gradient amplifiers in MRI drive the gradient coils with currents in excess of several hundred amperes to create the magnetic gradient field used in the imaging process. The magnetic gradient fields have to be modified at frequencies of up to a few kilohertz for fast imaging, and for the typical inductances of the coils on the range of several hundred microhertz to a millihertz, the voltages required are in excess of 1,500 V. The image quality and resolution depend greatly on how precisely controlled are

the applied fields. High performance systems require high accuracies on the currents to prevent image artifacts. The high power and high current accuracy required pose great challenges to the designer's selection of the power stage and the control. The reported solutions always involve structures with bridges in parallel or bridges stacked to be able to meet the requirements with the current existing semiconductor devices. Earlier solutions used linear amplifiers for their high fidelity but they became impractical for the power levels required nowadays. This led to hybrid solutions combining a linear amplifier, to provide the bandwidth and accurate control, with switched power stages to boost the voltage for the fast transitions. The linear amplifier stage becomes totally impractical for the high current levels of new systems. A solution proposed by Sabate et al. (*12*) consists of replacing the linear amplifier by a fast switching bridge (62.5 kHz) and two other bridges switching at lower frequency (31.25 kHz) to provide the higher voltage. The amplifier can be implemented with lower voltage ratings fast insulated gate bipolar transistor (IGBTs) on the high-frequency bridge and higher voltage rating but slower IGBTs for the low-frequency bridges. The interleaved operation of the three bridges provides a high-frequency low-amplitude ripple.

Claustrophobia has been an important concern that has been tackled by open MR systems. Another solution has been the development of shorter MRI machines, which has required the rebuilding of the engineering of the system. In particular the gradients are an important issue. If the area over which the wires are positioned is decreased, then the local power dissipation, which is related to the minimum wire separation and the hot spots of the coil, is increased. Gradient coil temperature is an important concern in the design and construction of MRI scanners (*13–16*).

To understand how acoustic noise is generated, consider a conductor element, **dl**, carrying a current, *I*, placed in a uniform magnetic field $\mathbf{B} = B\hat{\mathbf{k}}$. This will experience an Lorentz Force *F* per unit length given by:

$$\mathbf{F} = -\mathbf{B} \times I\mathbf{dl} = BI|\mathbf{dl}|\sin\theta\,\hat{\beta}, \qquad [15]$$

where θ is the angle between the conductor and the magnetic field, and $\hat{\beta}$ and $\hat{\mathbf{k}}$ are unit vectors which lie along the force and the magnetic field directions, respectively. *F* takes its maximum value when θ = 90°, and *F* = 0 when θ = 0°. Consider an element conductor d*l* of mass *m*, which is fixed via an elastic support to an immovable object, with spring constant, *k*. In real experiments, damping also has to be considered, the equation of motion for the system is given by:

$$F(t) = m\frac{d^2x}{dt^2} + \eta\frac{dx}{dt} + kx, \qquad [16]$$

where η is the damping constant. The solution of Eq. [16] indicates that the magnetic force of the conductor will accelerate it into a forced vibrational mode with displacement *x*. Mansfield et al. (*17*) proposed active acoustic screening for quiet gradient coils, minimizing the noise due to these displacements but reducing gradient strength. Wang and Mechefske (*18*, *19*) proposed a vibration analysis and testing of a thin-walled gradient coil model, the technique could predict the whole-body vibration modes of gradient coils in the low-frequency range allowing a reduction of the gradient noise.

All these requirements are based around the safety and comfort of the patient (*20–24*). The primary biological effect at frequencies of between 100 and 5,000 Hz (typical of MRI magnetic field gradient switching) is peripheral nerve stimulation, the result of which can be a mild tingling and muscle twitching to a sensation of pain. A typical modern clinical scanner is able to generate 40 mT m^{-1} at a switching rate of up to 200 T m^{-1} s^{-1}. Hence, the gradient can be switched from zero to maximum in 200 μs. Even higher values of gradient magnitude are usually desirable for diffusion-weighted imaging. Glover (*21*) recently published a review of the interaction of MRI fields gradient with the human body where explains in detail the low (audio) frequencies associated with the imaging gradient switching and the main response of PNS (Peripheral Nerve Stimulation), concluding that it is required a better understanding is required of how to relate nerve level thresholds to scanner settings in order to avoid PNS to either subjects or operators.

Applying rapidly switched magnetic field gradients can produce peripheral nerve stimulation in patients. This stimulation results from the electric field induced in tissues when the flux linked by the body changes. The heterogeneity of the body's electrical conductivity makes it difficult to produce a full modeling of the process of stimulation, but it is generally the case that the larger the peak magnetic field experienced by the body, the larger the induced electric field (see Fig. 3). The IRPA/INIRC Guideline on MRI (*25*) warns that electric field strengths exceeding 5 V m^{-1} may cause ventricular fibrillation, suggesting that the thresholds for nerve and cardiac muscle stimulation are very close to one another.

It is generally assumed in MRI that the magnitude of the total magnetic field is equal to the *z*-component of the field where in the presence of gradients G_x, G_y, and G_z

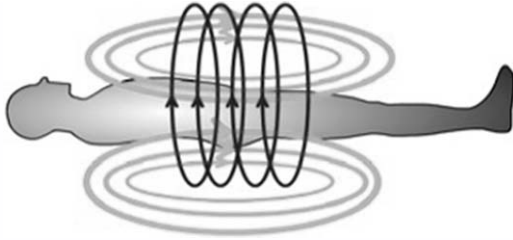$$B_z = B_0 + xG_x + yG_y + zG_z. \qquad [17]$$

Figure 3 Time varying gradient causes flux linked by body changes with time.

However, as a consequence of Maxwell's equations, the two transverse components, B_x and B_y, called "concomitant fields" or "Maxwell fields," are always generated at the same time when a gradient in B_z is generated. The magnitude of the total magnetic field is

$$B = \sqrt{B_x^2 + B_y^2 + B_z^2}. \qquad [18]$$

The value of the total magnetic field obtained inside the patient volume, when driving a given gradient coil axis (x, y, or z) dictates the potential for that gradient axis to induce peripheral nerve stimulation. The difference between the actual and the assumed magnetic field thus is

$$\Delta B_A = \sqrt{B_x^2 + B_y^2 + B_z^2} - B_z. \qquad [19]$$

The concomitant field components B_x and B_y can be computed from Maxwell's equations $\nabla \times \mathbf{B} = 0$ and $\nabla \cdot \mathbf{B} = 0$. When a gradient G_x is applied, a concomitant field component B_x is generated, which is given by

$$B_x = zG_x. \qquad [20]$$

When a gradient G_y is applied, a concomitant field component B_y is generated, which is given by

$$B_y = zG_y. \qquad [21]$$

Finally, when a gradient G_z is applied, two concomitant field components B_x and B_y are generated and are given by

$$B_x = -\frac{x}{2}G_z \qquad B_y = -\frac{y}{2}G_z. \qquad [22]$$

This behavior means that for all three types of gradient, one component of the field varies linearly with axial position. As the height of the human body is considerably greater than its breadth or width, it is generally the axially varying component of the field that produces the largest field magnitude in the body. In designing a gradient coil to allow higher rates of change of gradient with time, dG/dt to be produced at PNS threshold, it is therefore common practice to reduce the axial extent of the coil's region of linearity (26–28). For axial gradient coils, this works by limiting the peak magnitude of B_z in the body, while in the case of x- or y-gradient coils, it is the peak magnitude of the concomitant field that is limited. This approach however has the disadvantage of reducing the extent of the region over which imaging can be carried out.

Zhang et al. (29) conducted peripheral nerve stimulation experiments on human volunteers using four gradient coils of different DSV sizes. They found that the average peripheral nerve stimulation threshold increased as the diameter of the applied homogeneous gradient spherical volume (DSV) decreased; PNS parameters as minimum slew rate and ΔG_{min} varied inverse linearly with DSV; and, more surprisingly, chronaxie varied inverse linearly with the DSV. Zhang concludes that "chronaxie" cannot be considered to be a single value, nerve-specific constant. This work should help to design gradient coils considering both the DSV and the possible stimulation thresholds.

Hoffman and coworkers (30) found a dependency of stimulation threshold on patient positioning and PNS. According to their studies, a generalization of the absolute stimulation thresholds is difficult because the gradient systems of different manufacturers differ (e.g., the region of maximum gradient flux density). Therefore, stimulation thresholds should be adapted to the respective gradient system.

Limiting the region of linearity using a modular gradient coil concept has been described by Harvey and Katznelson (26) as a method of avoiding peripheral nerve stimulation.

The study of electric fields induced in the human body by time-varying magnetic field gradients in MRI have been constantly studied for creation of new techniques where PNS could be avoided. Bencsik et al. (31) propose the study of the variation of electric and magnetic field using MAFIA and a three-dimensional HUGO body model, to make predictions according to the variation of the rate of change of gradient in the three gradients x, y, and z, and they have shown that the induced electric field is strongly correlated to the local value of resistivity.

For now, FDA (Food and Drug Administration) has limited perfectly the safe limits to avoid PNS in patients. More studies of PNS are required to understand the process between PNS not just in cylindrical coils but in planar and the new geometries that are now investigated (32).
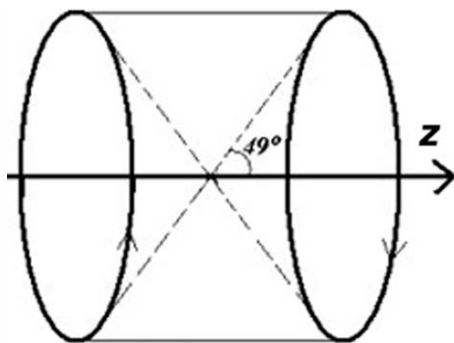
Figure 4   A Maxwell coil.

IV. METHODS FOR GRADIENT COIL DESIGN

Gradient coils can be made of discrete wires or distributed wires arranged on a cylindrical surface. Coils of both forms are described in this section.

Coils With Discrete Windings

The discrete-wire coils are made of hoops and saddles positioned strategically so as to produce a magnetic field gradient. The magnetic field due to a wire arrangement can be described using a set of complete orthogonal functions (spherical harmonics). In designing a discrete-wire gradient coil, the saddle or hoop positions are chosen to eliminate unwanted high-order harmonics leaving the low-order harmonic corresponding to the desired field gradient (33–35).

The Maxwell coil pair consists of two circular hoops of radius, a, carrying currents circulating in opposite directions, spaced by a distance of $\sqrt{3}$ of the hoop radius, a. This spacing eliminates the unwanted spherical harmonic terms, which produce fields varying as z^3 and $z\rho^2$ (in cylindrical coordinates) The field gradient from the Maxwell coil is uniform to 5% within a sphere of radius 0.5 a at the center of the gradient coil, and the efficiency is (5) $\eta = 8.058 \times 7 / a^2$T m^{-1} A^{-1}. The gradient uniformity rapidly worsens at spherical radii greater than 0.5 $\times$ a (see Fig. 4).

Figure 5 shows a Golay coil, which generates a y-gradient. It consists of eight straight wires running parallel to the z axis, with four inner arcs and four outer arcs that provide return paths. As current flow in the wires running parallel to the z axis does not produce a z-component of the magnetic field, these wires do not affect the field gradient. The position of the arcs and the angle that they subtend are chosen so

as to eliminate unwanted spherical harmonics in the field expansion.

The Golay coil's homogeneity can be improved by using more arcs with different arc lengths placed at different positions so as to eliminate higher order terms in the field expansion (34). Some examples of such coils are given in papers by Frenkiel et al. (36), Suits (37), and Siebold (38). An x-gradient coil is generated by a rotation of the entire set of four saddle units by 90° about the z axis.

Coils With Distributed Windings

The existence of high-order azimuthal or tesseral harmonics, which arise from the small number of wire positions involved and the filamentary nature of the currents are one problem of gradient coils with discrete wire paths (Fig. 6). Such coils also tend to have poor values of η^2/L. The idea of using a continuous current distribution on the surface of a cylinder is to obtain considerably larger usable volumes (13). Different methods have been developed for finding optimal positions for the multiple windings: matrix inversion techniques, "stream function" methods, the target field approach developed by Turner (8), the harmonic minimization approach introduced by Carlson et al. (9), wave equation technique for compact gradient coils (39), momentum-weighted conjugate gradient descent (MW-CGD) algorithm that uses a type of nonlinear constrained optimization (40), simulated annealing (SA), which is a stochastic optimization strategy (41–43).

Matrix Inversion Methods.   These methods are related to finite element methods. They allow the use of any shape of coil former but require long computation times. The idea of these methods is to give a very uniform magnetic field over a matrix, which describes the magnetic field at N different locations. If N such points are well chosen, the matrix may be invertible, giving a set of currents at N positions on the coil former, which may then be approximated by piling up appropriate numbers of turns at these positions. Hoult (44) suggested in 1977 that a solenoid could be opti-
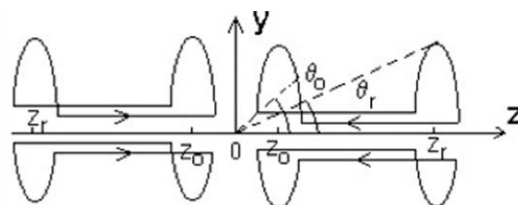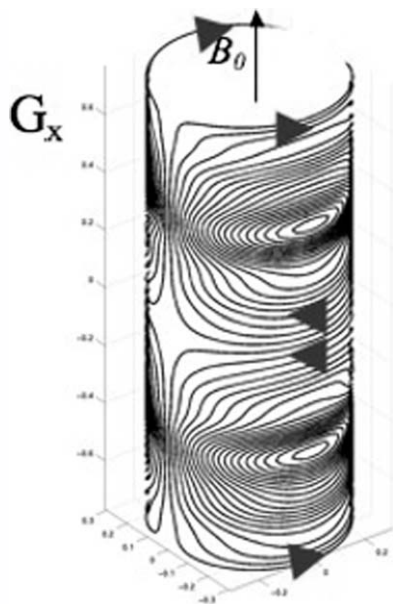

Figure 5   A Golay coil.

Figure 6   Illustration of the *y*-gradient coil windings.

mized to give a very uniform field using this approach. In practice, a coil designed using this method requires large variations in current from one turn to the next. More improvements were made by Compton (*45*) who developed a distributed-arc coil design giving gradients departing from the desired characteristics by a predetermined error. Schweikert et al. (*46*) calculated optimized currents at specific surface elements, and Wong et al. (*47*) proposed an approach in which the current and the number of turns are kept fixed, while the current element position is allowed to vary. A benefit of this type of coil design method is that there is no stage of approximation between a calculated continuous current density and the practical realization of discrete current carrying wires. However, the field from an array of wires approximating a current sheet converges very rapidly to that of the current sheet as the number of wires increases: as few as 20 turns may be required (*5, 7, 8*).

"Stream Function" Methods.   The stream function $I(z, \phi)$ on a cylinder is that function which, if differentiated with respect to z or ϕ, gives the current density in the azimuthal or axial direction, respectively. The wires of a coil which approximate the current distribution are located at equally spaced contours of the stream function.

Target Field Method.   In the target field method, Ampere's law is inverted to calculate the currents required directly from the specification of the desired field variation. The target field method has been the most popular gradient coil design method due to

their computational ease in determining a suitable wire pattern (Fig. 7). Turner (*4–6, 8*) prescribes a desired (or target) magnetic field over the cylindrical surface inside the cylindrical gradient coil. A current distribution is calculated over the surface of the gradient coil to achieve the targeted magnetic field. Also in the theoretical development the inductance in terms of the current distribution is minimized subject to the magnetic flux density and to a desired field distribution in the region of interest (ROI).

Harmonic Minimization Approach

Although the target field and minimum inductance approach can be simply modified for use with screened coils, a different method, based on the work of Carlson et al. (*9*), was used for designing screened coils in the work of this review. This method is better suited to designing coils of constrained length than the minimum inductance method (*4*). There are other methods that consider the low inductance for a gradient system of restricted length [Chronik and Rutt (*48*) and Andrew and Szcesniak (*16*)]. Next subsection presents an example of the mathematical machine for a *z*-gradient coil, a similar development can be reproduced for *x*- or *y*-gradient coil design that could be an exercise for students.

z-Gradient Coil.   Consider that the current distribution on the inner cylinder is limited to the region $|z| < l$. Considering a *z*-gradient coil, the inner coil current distribution is defined as a weighted harmonic series (*4, 8, 9, 49*),

$$\begin{aligned} j_\varphi &= \sum_{n=1}^{N} \frac{\lambda_n}{2l} \sin\left(\frac{\pi n z}{l}\right) \quad |z| < l \\ j_\varphi &= 0 \qquad\qquad\qquad |z| > l \end{aligned} \quad [23]$$

Fourier transformation of Eq. [23] yields,

$$j_\varphi^0(k) = \sum_{n=1}^{N} i\lambda_n[\text{sinc}(kl - n\pi) - \text{sinc}(kl + n\pi)] \quad [24]$$

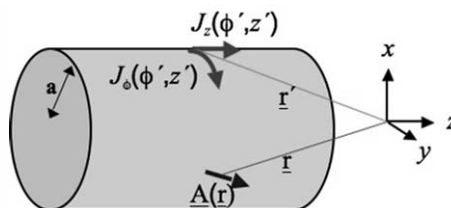where $\text{sinc}(x) = \sin(x)/x$. Defining $\chi = ka$, Eq. [24] becomes,

Figure 7   Current distribution, $J(\varphi, z)$ on cylinder of radius, a.

$$j_\varphi^0(\chi) = \sum_{n=1}^{N} i\lambda_n \left[\mathrm{sinc}\left(\frac{\chi l}{a} - n\pi\right) - \mathrm{sinc}\left(\frac{\chi l}{a} + n\pi\right) \right]$$

$$[25]$$

and the magnetic field in the region $\rho < a$ depends on $j_\phi^0(\chi) = i \sum_{n=1}^{N} \lambda_n j_n(\chi)$ and can be written as

$$B_z(r, \varphi, z) = \frac{\mu_0}{2\pi a} \int_{-\infty}^{\infty} \chi d\chi j_\varphi^0(\chi) e^{(i\chi\frac{z}{a})} I_0(\chi\frac{r}{a}) K_1(\chi) \quad [26]$$

where

$$j_n(\chi) = \left[\mathrm{sinc}\left(\frac{\chi l}{a} - n\pi\right) - \mathrm{sinc}\left(\frac{\chi l}{a} + n\pi\right) \right]. \quad [27]$$

The magnetic field can be written as

$$B_z(r, \varphi, z) = \sum_{n=1}^{N} \lambda_n b_n \quad [28]$$

b_n has the form

$$b_n = \frac{\mu_0 i}{2\pi a} \int_{-\infty}^{\infty} d\chi \, e^{i\chi\frac{z}{a}} \chi j_n(\chi) K_1(\chi) I_0(\chi\frac{r}{a}) \quad [29]$$

while the inductance is given by:

$$L = \frac{\mu_0 a^2}{I^2} \int_{-\infty}^{\infty} dk \left| j_\varphi^0(\chi) \right|^2 I_1(\chi) K_1(\chi) \quad [30]$$

This equation can be used to evaluate the performance of a coil design. To design a coil, a functional made up of the sum of the squares of the field deviation from the desired field variation, $B_z = gz$, over a set of N_p points, added to the inductance weighted by a factor, α, is minimized:

$$U = \sum_{q=1}^{N} \left(gz_q - B_z(r_q) \right)^2 + \alpha L. \quad [31]$$

Minimization requires that

$$\frac{dU}{d\lambda_p} = \sum_{q=1}^{N} 2\left(gz_q - B_z(r_q)\right)\frac{dB_z(r_q)}{d\lambda_p} + \alpha\frac{dL}{d\lambda_p} = 0 \quad [32]$$

which can be evaluated using

$$\frac{dB_z(r_q)}{d\lambda_p} = b_q(r_q) \quad [33]$$

$$\frac{dL}{d\lambda_p} = \frac{2\mu_0 a}{I^2} \int_{-\infty}^{\infty} d\chi \sum_{n=1}^{N} \lambda_n j_p(\chi) j_n(\chi) I_1(\chi) K_1(\chi). \quad [34]$$

This yields N simultaneous equations involving the N coefficients of the form

$$a_n = c_{11}\lambda_1 + c_{12}\lambda_2 + \dots + c_{N1}\lambda_N \quad [35]$$

which can be written in matrix form

$$\mathbf{a} = \underline{\underline{\mathbf{C}}} \cdot \underline{\boldsymbol{\lambda}} \quad [36]$$

$$a_p = 2g \sum_{n=1}^{Q} z_q b_\mathrm{p}(r_q) \quad [37]$$

with matrix elements:

$$c_{pm} = \sum_{q=1}^{Q} 2b_p(r_q) b_m(r_q)$$

$$+ \alpha \frac{2\mu_0 a}{I^2} \int_{-\infty}^{\infty} d\chi j_m(\chi) j_p(\chi) I_1(\chi) K_1(\chi). \quad [38]$$

This set of equations can be solved by Gaussian elimination to yield the optimal coefficients, λ_n.

Having solved Eq. [36] to find the optimal λ's, the current distribution is then given by Eq. [36]. The azimuthal symmetry of the current distribution means that the coil will be composed of an array of a wire loops. The loop positions, z_n, which best represent this distribution are given by

$$I_n = \int_0^{z_n} j_\varphi dz' = \frac{(2n-1)}{2N} \int_0^{\infty} j_\varphi dz'. \quad [39]$$

It has been mentioned that η^2/L should be as large as possible whilst keeping the gradient homogenous. To find the efficiency, the value of Eq. [51] must be evaluated at the origin

$$\frac{dB_z}{dz} = \frac{i\mu_0}{2\pi a^2} \int_{-\infty}^{\infty} \chi^2 d\chi j_\varphi^0(\chi) e^{(i\chi\frac{z}{a})} I_0(\chi\frac{r}{a}) K_1(\chi). \quad [40]$$

Evaluating at the origin, $I_0(\chi\frac{r}{a}) \to 1$ as $r \to 0$ and $e^{i\chi\frac{z}{a}} \to 1$ as $z \to 0$ only $\cos(\chi\frac{z}{a})$ contributes because $\chi^2 j_\varphi^0(\chi) I_0(\chi\frac{r}{a}) K_1(\chi)$ is symmetric. The efficiency is given by:

$$\eta = \frac{\mu_0}{2\pi a^2 I} \int_{-\infty}^{\infty} d\chi \chi^2 j_\varphi^0(\chi) K_1(\chi) \quad [41]$$
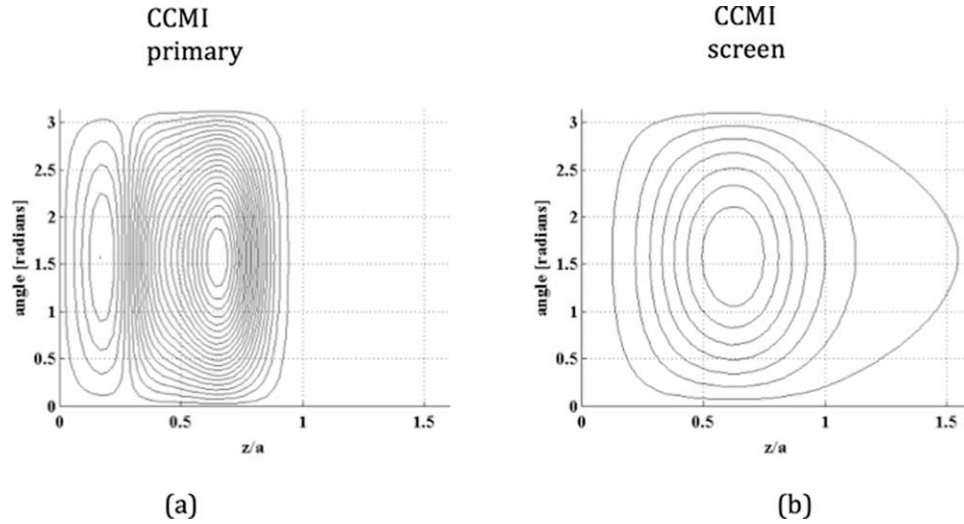
Figure 8 Wire patterns for shielded gradient coils with aspect ratio =1 that achieved z-ROU = 45% (a) primary coil by CCMI (b) screen coil by CCMI.

and

$$\frac{\eta^2}{L} = \frac{\mu_0}{4\pi^2 a^5} \frac{\left[\int_{-\infty}^{\infty} d\chi \chi^2 j_\varphi^0(\chi) K_1(\chi)\right]^2}{\int_{-\infty}^{\infty} dk \left|j_\varphi^0(\chi)\right|^2 I_1(\chi) K_1(\chi)}. \qquad [42]$$

Constrained Current Minimum Inductance Target Field Method

Chronik's paper developed the idea of the constrained current minimum inductance target field method (CCMI), proposed by Turner (5, 48, 50–52). These constraints allow a longer region of uniformity for a shorter gradient coil. The first constraint is related to the z-component of the magnetic field. The second current constraint is the closure constraint that prevents any current density from crossing the boundaries of a specified area on the surface of the cylindrical former. The third current constraint forces the current density to remain constrained within some region of the coil surface using the values of the azimuthal current density over a set of coordinates. Once the constraints have been identified, the functional to be minimized takes the form

$$U\left(j_\phi^m(k)\right) = L\left(j_\phi^m(k)\right) + \sum_{n=1}^{N} \lambda_n[B_z - B_{zn}]$$

$$+ \sum_{n=1}^{P} \lambda_p\left[J_\phi - J_{\phi p}\right] + \lambda_q\left[\Lambda_\phi - \Lambda_q\right] \quad [43]$$

where $j_\phi^m(k) = \sum_{n=1}^{N} \lambda_n a_n^m(k) + \sum_{p=1}^{P} \lambda_p a_p^m(k) + \lambda_q c_q^m(k)$.

Figure 8 shows wire patterns for shielded gradient coils with aspect ratio =1 that achieved z-ROU (Region of Uniformity) = 45% (a) primary coil by CCMI (b) screen coil by CCMI.

Boundary Element Method

Unconventional coil structures have been explored with the help of advanced numerical algorithms such as the boundary element method (BEM) (53–56), during the numerical implementation, the relationship of the targeted fields over the DSV and shielding, and the current's source is first determined by applying BEM representation of Biot-Savart's integral equation, then an inverse solution is sought for the current density distribution. Pissanetzky (57) proposed the inverse boundary element method (IBEM) and applied the method for design gradient coils on an arbitrary surface minimizing the stored energy and inductance. Lemdiasov and Ludwig, who included a torque minimization, demonstrated a matrix inversion algorithm to obtain the solutions. Most significant is the work of Peeren (58) who used power dissipation and stored energy and who also demonstrated how to impose active magnetic screening by minimizing the magnetic field of the eddy currents rather than minimizing the flux that escapes onto the cryostat.

Recently, Poole and Bowtell (54) added to this idea the minimization of power dissipation in terms of a current distribution. The functional Φ contains the addition of the weighted power loss term, βP, and removal of the field offset term, $\mathbf{B}_z^{\text{off}}$.
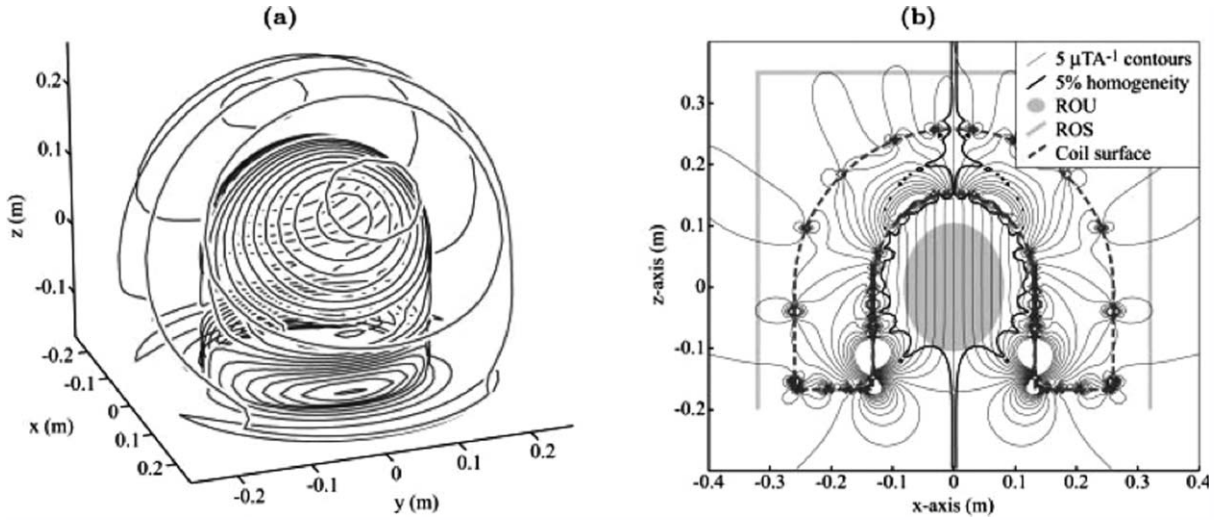
Figure 9   Shielded head gradient coil using the inverse boundary element method.

$$\Phi = \frac{1}{2} \sum_{k=1}^{K} W(\mathbf{r}_k) \left[B_z(\mathbf{r}_k) - B_z^t(\mathbf{r}_k) \right]^2 + \frac{\alpha}{2} L$$
$$+ \beta P - \lambda_x M_x - \lambda_y M_y - \lambda_z M_z \quad [44]$$

To impose active magnetic screening in the Peeren contribution, an extra term can be added to this equation that is the sum of squares of the eddy-current-induced magnetic field. Proposing another functional (Eq. [44]), the minimization of the difference between the target field and actual field, the stored energy, the power loss and the imposed torque balancing. The interesting contribution is that the mesh elements allow mapping in 3D space and take care of the minimum wire spacing to ensure feasible coils. Adding an extra term can be used to lower the maximum current density magnitude. Poole et al. (*54*, *55*, *59*) present different coils designs for head imaging, ultra short gradient coils, shoulder-slotted gradient coils, and shielded head gradient coils (Fig. 9). In general, it can be noticed that increasing the number of elements gives a better approximation of the continuous current density, but this comes at the cost of increased computation time. The main advantage of these methods is that the coil space can be arbitrary thus allowing greater flexibility than the conventional methods. The BEM has also been combined with the equivalent magnetization current method to design the gradient coils (*15*). However, two main drawbacks have been identified in these sorts of numerical algorithms, although this is an ill-posed problem in mathematics, Shou et al. (*60*) proposed a solution that this is discussed on the next section.

Regularization of Ill-Posed Problems

Ill-posed problems are frequently encountered in science and engineering. The term itself has its origins in the early 20th century. It was introduced by Hadamard who investigated problems in mathematical physics. According to his beliefs, ill-posed problems did not model real-world problems but later it appeared how wrong he was. Hadamard defined a linear problem to be well posed if it satisfies the following three requirements: a) existence, b) uniqueness, and c) stability. A problem is said to be ill posed if one or more of these requirements are not satisfied (*61–63*). In the case of designing gradient coils, it has been found that the target field causes the system to be ill posed; quite different current densities may generate almost identical magnetic fields. The system of equations used to design gradient coils forms an ill-posed inverse problem in which the number of solutions is infinite. Some solutions have been proposed to convert this problem into one that is well-posed. The most common of these is Tikhonov regularization (*62*, *63*), which additionally minimizes the least-squares norm of the solutions. Poole (*54*) converts into a well-posed problem using BEM with minimizing the power dissipation. BEM and Finite Element Method (FEM) methods are ill-posed problems and severally questioned because the solution cannot be found directly. Inductance and torque are introduced to constrain the optimal solution space. In general, this is computationally expensive and sometimes no numerical solution can be found. Another problem of the BEM- or FEM-based methods is that the direct numerical assumptions used lead

to unrealizable coils in engineering, e.g., sometimes it will introduce dense wires into the design, which would generate severe heating problems. Shou et al. (60) attempt to improve the BEM method for MRI coil designs by applying the Tikhonov regularization scheme to solve the ill-posed matrix system formulated by the BEM forward model to build biplanar transverse gradient coils. Shou et al. (60) transformed practical engineering constraints into the numerical boundary conditions and then applied it into the BEM formulation.

Peripheral Nerve Stimulation and Gradient Coil Design

Peripheral nerve stimulation limits the use of whole-body gradient systems capable of slew rates >80 T m^{-1} s^{-1} and gradient strengths >25 mT m^{-1}. The stimulation threshold depends mainly on the amplitude of the induced electric field in the patient's body, and thus can be influenced by changing the total magnetic flux of the gradient coil (21, 23, 64). Kimmlingen et al. built a system that consists of a modular six-channel gradient coil designed with a modified target field method, two three-channel amplifiers, and a six-channel gradient controller. It is demonstrated that two coils on one gradient axis can be driven by two amplifiers in parallel, without significant changes in image quality (27). Allowing continuous variation of the field characteristics to permit the use of full gradient performance without stimulation (slew rate 190–210 T m^{-1} s^{-1}, G_{max} 32–40 mT m^{-1}).

Promising structures as the multilayer gradient coils (65) could be a solution to reduce PNS in the human head, with a minimum net torque. This seems possible once this is an asymmetric gradient coil where negative turns are generated at the coil entrance.

The model of using an efficient multiple field of view gradient coil set prevents PNS using three different field-of-views (FOVs) according to the necessities: body, cardiac, and brain mode. The gradient coil set uses the full power of a single gradient power supply in all three operating modes (66). Goodrich and co-workers (67) built and tested of a two-region gradient coil insert as a proof of concept for an extended FOV, contiguous, three-region human-sized gradient system. When combined with an overlapping single-region gradient insert, extended FOV imaging will be possible without moving the table or the subject and without increasing nerve stimulation. This system requires an RF system for each view, so, it becomes more challenging to adapt new hardware for this novel idea.

Torque

Nontorque balance of a transverse gradient coil occurs when axial symmetry is removed, i.e., it will experience a net torque when carrying a current in the presence of a large static magnetic field. It is therefore necessary to take special steps in the design process to ensure that the wire paths are arranged so as to yield zero torque and force (68). Alsop and Connick (69) present an optimization of torque-balanced asymmetric head gradient coils (70), comparing gradient coils of various lengths both with and without torque constraints; concluding that asymmetric torque-balanced coils can achieve comparable homogeneity with only a modest increase in inductance and resistance. New geometric designs require special care to be taken on this issue. Liu and Petropoulos (71) described the design of spherical z-gradient coil using minimum inductance approach. Green et al. (72) took the hemispherical gradient coil idea and adds a term where consider the total torque formed from a stream function (77). When this is not considered, the net torque makes its operation at high currents and fields problematic, although this inclusion of torque-balancing produces a considerable reduction of the performance of the transverse hemispherical coils, as is also the case for asymmetric, cylindrical coils. Other example is the case of asymmetric head gradient coil, where a reduction of up to 80% in net torque only decreases the figure of merit by 5% from its maximum value. Torque reductions larger than 80% can produce solutions with poor coil performance (65).

V. SHIELDED GRADIENT COILS

The interaction of the rapidly switched gradient fields with other conducting structures in the MRI system is the main cause of eddy currents (Fig. 10). These eddy currents generate magnetic fields, which cause problems in imaging (6, 9, 50, 73–83). One solution was proposed by Martens et al. (84) and Van Vaals et al. (85). The idea is to adjust the current waveform applied to the gradient coils so as to produce a field variation which when combined with the eddy current–induced fields produces the desired field variation with time. Morich et al. proposed doing this by extracting the properties (amplitudes and decay time constants) of intrinsic eddy current–induced magnetic fields generated in the MRI system when pulsed field gradients are applied. This approach is known as pre-emphasis.
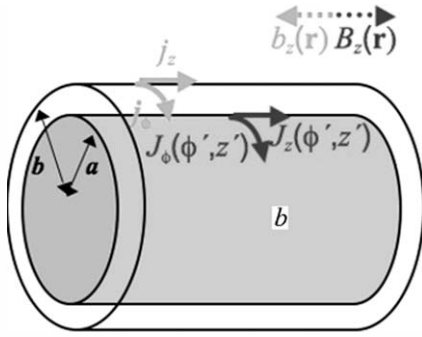
Figure 10 Geometry of a screened gradient coil: inner coil cylinder (radius a) with screen (radius b). Add second coil [$j(\varphi, z)$] on external cylinder of radius, b ($b > a$).

A better approach is to use screening to eliminate the interaction that causes eddy currents to be generated in the first place. Turner and Bowley (6) proposed the use of passive shielding to eliminate eddy currents; the idea is to place a shield between the gradient coils and the surrounding conducting structures, thus canceling the gradient magnetic field outside the shield. The thickness of the shield must be greater than the skin depth at gradient-switching frequencies. In this case, the time dependence of the field produced by the eddy currents in the shield may not however be the same as that of the gradient coil current. A better way to avoid eddy currents is therefore to design gradient coils that do not produce a magnetic field outside the coils. Such coils must consist of at least two coil windings on cylinders of different radii. This technique is referred to as active shielding or self-shielding [Mansfield (73–75, 86); Roemer and Hickey (76); and Bowtell and Mansfield (77)]. The technique is described in detail below, taking advantage that the target field has already been described for gradient coil design. This approach may be used to design actively screened gradient coils. In a screened cylindrical coil, a second coil cylinder surrounding the first is introduced. The wires in this second screening coil are positioned so as to cancel the field from the inner coil in the region outside the screen. There will be a decrease in coil efficiency for a given inductance, but the inductive coupling with surrounding conductive structures is eliminated (Fig. 8).

It is important to mention that the price paid for magnetic screening is therefore reduced coil efficiency at fixed inductance (78). Connecting the screen and primary coils in series guarantees the temporal variation of current in the two coils is identical so that screening takes place at all times whilst a gradient waveform is being played out.

VI. APODISATION

Minimizing the coil inductance can cause the current distribution to become oscillatory, which makes fabrication of the coil problematic. This behavior becomes more severe as the coil length is shortened. The most rapidly varying current components can be removed by apodisation (5). This involves multiplying $j_\phi(k)$ by a Gaussian function, $e^{-2k^2 h^2}$, where h is the apodisation length, which offers an additional degree of freedom for customizing a coil for particular experimental requirements. The effect of apodisation lengths of about one-tenth of the coil radius is to smooth out the field variation, reducing the inductance slightly, and removing the undesirable current density oscillations.

VII. PLANAR GRADIENT COILS

An interesting geometry in the design of gradient coils is the planar design. Planar gradient coils provide an interest to researchers due to their ability to be separated and also because the DSV contained between the plates is more accessible (87–96). The DSV is the region in which a quality image can be obtained and it should be as large as possible for a given plate size. The techniques that are used to build this kind of gradient coil can be the target field method, the minimum inductance, wave equation, and minimum power techniques. Vegh et al. (93, 94) proposed the use of the wire path correction with optimized variables allowing high magnetic gradient field strengths and large imaging regions can be obtained for planar gradient coils (Fig. 11). Forbes et al. proposed the use of a target field method to design circular biplanar coils for asymmetric shim and gradient fields, noticing that a closer agreement between the computed and target field comes at the cost of more elaborate winding patterns with more regions in which the current is reversed. This is likely to be the limiting factor on how accurately the target field can be reproduced, in terms of practical manufacture of the coils of any geometry (97). Liu et al. (98–100) used a variation of the target-Carlson method to build biplanar gradient coils, aware that this is an ill-posed problem, depending on the choice of the target-field points. Their numerical simulations showed that if the target-field points are set in the first octant, the problem is not ill posed. Therefore, it is possible to get desired solutions easily using matrix software instead of the standard Tikhonov regularization method.
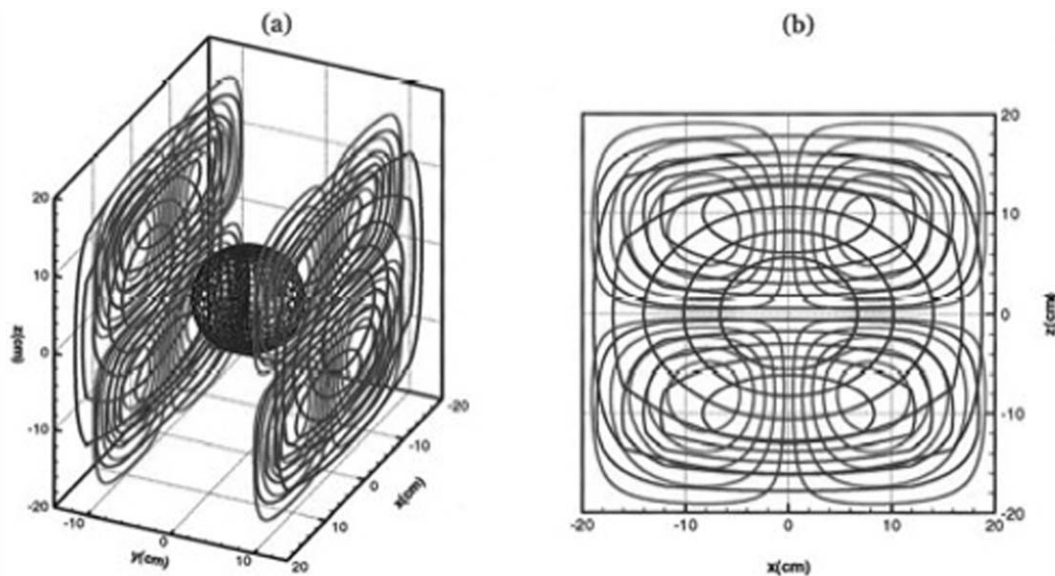
Figure 11   Design proposed by Vegh et al. (a) Planar gradient coil design and associated DSV (black sphere) and (b) example of overlapping windings of *x*, *y*, and *z* gradient coils.

Vegh et al. (*39*) proposed a wave equation method for the design of gradient coils which is novel within the field. The proposed wave equation technique for gradient coil design has been compared with the state-of-the-art target field method. It was shown that using the proposed method of design, smaller gradient coils can be obtained with comparable specifications. The new design methodology allows the design of gradient coils for special purpose imaging that may require larger gradient field strengths and it takes 12 h to optimize a coil.

VIII. GRADIENT COILS DESIGN MOTIVATED BY NEW COMBINED TECHNIQUES

New combined techniques such as spect-mri, ultrasound-mri, positron emission tomography-magnetic resonance imaging (PET-MRI) present a challenge to develop compatible hardware between these techniques without affecting the performance of each technique. Plewes et al. (*101*) present a work of imaging ultrasound fields, based on the use of a single gradient axis that allowed motion detection in one direction and also (by aligning the gradient with the US propagation direction) allowed clear visualization of the field properties. However, extension to the use of multiple gradients, while more complex, is clearly possible and would provide the full vector field of motion.

PET–MRI technique has demonstrated to be a powerful tool of diagnostic, combining the excellent spatial resolution provided by MRI and on the other hand the small changes in metabolite concentrations detected by PET. Pichlet et al. (*102*) in their review discuss the many technical challenges, including possible interference between these modalities, which have to be solved when combining PET and MRI and various approaches have been adapted to resolve these issues. Pichlet presents an overview of current working prototypes of combined PET/MRI scanners from different groups. In addition, besides PET/MR images of mice, the first such images of a rat PET/MR, acquired with the first commercial clinical PET/MRI scanner, are presented on his work. The combination of PET and MR is a promising tool in preclinical research and will certainly progress to clinical application. MRI and PET scientists have made a big effort to make this possible. One problem to solve is that multiplier tubes used in PET are sensitive to magnetic fields. Pichler et al. (*103*) proposed to build a PET detector to fit inside the standard gradient set.

Poole et al. (*104*) designed a novel set of gradient and shim coils specially designed for split MRI scanner to include an 110-mm gap from which wires are excluded so as not to interfere with positron detection. An IBEM was necessarily used to design the three orthogonal, shielded gradient coils, and shielded Z0 shim coil. The coils have been constructed and tested in the hybrid positron emission tomography-MRI system and successfully used in simultaneous positron emission tomography-MRI experiments.

IX. OTHER GEOMETRIES AND NECESSITIES

New geometries are continually being investigated, through the innovation of new methods or by optimizing the existing ones (*105*, *106*). Computers have evolved, with a considerable calculation time decrease, allowing the optimization of old methods that appeared to be obsolete. This search is a consequence of the new advances in MRI such as functional MRI [echo planar imaging (EPI)] (*11*, *71*), diffusion, perfusion, cellular imaging, and short clinical systems (*19*) and of the need for solutions to unsolved problems such as claustrophobia, NMR microscopy (*95*), and PNS (*106*). There are some promising results with new geometries Poole et al. (*54*). Open MRI systems usually use vertical-field magnets because interventional studies can be performed more conveniently with them. The use of convex-surface gradient coils for a vertical-field open MRI system has been proposed to obtain stronger gradient field strength with a smaller coil inductance while maintaining enough space for interventional operations. The convex-surface gradient coils are designed using the finite element method where the convex surfaces are defined at the prolate spheroidal coordinate (*107*). Noisy gradients require new measures to reduce the noise. Forbes used an analytical approach to the design of quiet cylindrical asymmetric gradient coils, for computing the deflection of a cylindrical gradient coil because of Lorentz forces, and for incorporating this into an optimization strategy for coil design. However, there is a trade-off between acoustic noise reduction and the accurate matching of the target field, so that a practical limit exists to the amount by which noise can be reduced within conventional coil geometry.

Lemdiasov et al. (*53*) propose a variation of the stream function approach; this method involves discretizing the surface into triangular elements, and then using a current flow formulation, which involves a constraint cost function including the desired field in a particular ROI in space and the stored energy. Tomasi (*108*) shows that for the cylindrical geometry, the fast SA method can be used to optimize the stream function used to design short gradient coils, using an optimum stream function with an emphasis near the coil end to give a coil-end correction. This approach has the advantage that the optimum stream function can be used to develop gradient coils with different numbers of wires, with different efficiencies and inductances but similar homogeneous gradient volumes. The results were compared with those corresponding to target field (TF) designs, and show that for short coils, the FSA designs exhibit larger homogeneus gradient volume (HGV) and lower coil inductance than those resulting from the TF method, while demonstrating similar efficiency. Rostilav et al. present a theoretical formulation that involves a constraint cost function between the desired field in a particular ROI in space and an almost arbitrarily defined surface that carries the current configuration based on Biot-Savart's integral equation. The theoretical model is formulated in a form that makes it applicable to a wide variety of shapes and geometries design (*92*).

Haywood presents a model three-axis gradient coil incorporating active acoustic control, which is applied to the switched read gradient during a single-shot rapid EPI sequence at a field strength of 3.0 T. This has been used to produce a snap shot image using EPI with an imaging time of 10.6 ms. The acoustic noise reduction measured over the specimen area is ~40 dBA as presented or ~34 dBA if the acoustic control winding is not activated.

Wang and Mechefske (*18*, *19*) presented a complete study looking at the cylinder reference surface, the cylinder thickness, the cylinder supports, and the cylinder materials. In the low-frequency range, the cylinder reference surface is the most significant factor. The magnitude of forcing functions are not only determined by the current and the magnetic strength but also affected by the coil spatial distribution.

Ruset et al. (*109*) present an open MR system for lung imaging at low fields, with a very particular specifications: planar gradient coils that generate gradient fields up to 0.18 G cm^{-1} in the x and y direction and 0.41 G cm^{-1} in the z direction. Gradient line filtering was a special challenge given the proximity of the desired bandpass frequencies (1–2 kHz) and those to be filtered (50–200 kHz). The slew rate of the readout gradient amplifier was slower than the others because the attached z-gradient coil possessed a greater inductance than the others, causing the shapes of each pulse to be slightly distorted on rise and fall.

In standard cylindrical gradient coils consisting of a single layer of wires, a limiting factor in achieving very large magnetic field gradients is the rapid increase in coil resistance with efficiency. A good level of screening can be achieved in multilayer coils (*81*, *110*), and small versions of such coils can yield higher efficiencies at fixed resistance than conventional two-layer (primary and screen) coils, and that performance improves as the number of layers increases. Simulations showed by Legget et al. (*81*) showed that by optimizing multilayer coils for cooling it is possible to achieve significantly higher gradient strengths at a fixed maximum operating temperature.

MRI gradient coil design is a type of nonlinear constrained optimization. A practical problem in transverse gradient coil design using the CGD method is that wire elements move at different rates along orthogonal directions. A MW-CGD method is used to overcome this problem. Jesmanowicz et al. take advantage of the efficiency of the CGD method combined with momentum weighting, which is also an intrinsic property of the Levenberg-Marquardt algorithm, to adjust step sizes along the three orthogonal directions. Experimental data demonstrate that this method can improve efficiency by 40% and field uniformity by 27%. This method has also been applied to the design of a gradient coil for the human brain, using remote current return paths. The benefits of this design include improved gradient field uniformity and efficiency, with a shorter length than gradient coil designs using coaxial return paths (40, 47).

Elliptical cross section asymmetric transverse gradient coils has been proposed by Crozier, the method is based on a flexible stochastic optimization method and results in designs of high linearity and efficiency with low switching times. The advantages of the modified SA are the simple mathematics used and that the calculations are performed on actual wire or sheet positions rather than current densities, allowing a realistic impression of the performance of the designs (111).

Forbes et al. (112) present a simplified, linearized model for the deflection of the coil due to electromagnetic forces, which is amenable to solution using analytical methods. Closed-form solutions for the coil deflection and the pressure pulse and noise level within the coil are obtained with his method. These are used to design new coil winding patterns so as to reduce the acoustic noise. Sample results are shown both for unshielded and shielded gradient coils. Extensions of this model are indicated, although it is suggested that the advantages of the present closed-form solutions might then not be available, and fully numerical solutions may be required instead.

3D gradient coils is other possibility to improve the performance of gradient coils for ultra short MR systems. The challenge is to reduce system length while maintaining performance, e.g., to maintain acceptable linearity and uniformity over a large field of view (FoV). Zhang et al. discusses the finding that the shortest systems have forced a reappraisal of the minimum requirements for shielded and unshielded gradient coil system as the lower inductance, minimum length coil, maximum efficiency and coil diameter to be able for achieving greater region of linearity and faster switching gradient coil to improve the quality of the image (113). Shvartsman's design of short cylindrical gradient coils with 3D current geometry introduces the concept of a conical surface for current flow, and does not require truncation of the shield current density (24, 83).

Toroidal surfaces concept has been introduced by Crozier and coworkers (114). This novel geometry is based on previous work involving a 3D current density solution, in which the precise geometry of the gradient coils was obtained as part of the optimization process. Regularization is used to solve for the toroidal current densities, where by the field error is minimized in conjunction with the total power of the coil. The utility of the third radial dimension can potentially lead to additional novel and interesting coil geometries to the toroidal structures. The method has the added advantage of being semianalytical and hence, fully tractable and computationally nonintensive, although it requires more work analyzing acoustic noise, peripheral nerve stimulation, and thermal performance.

X. SUMMARY

The necessity to produce large, rapidly switched magnetic field gradients has been a prerequisite for looking at new methods for the design of gradient coils that allow the implementation of many high-speed imaging techniques as fMRI, diffusion, perfusion, and cellular imaging. The perfect gradient coil has not been built yet, but recent techniques have allowed decreasing power consumption, inductance, stored energy, heating, and resistance, improving the ROI and SNR. The new approach is to build short gradient coils that allow reduced scan time, improving the SNR.

The constant search for better gradients coils, with different geometries is still the motivation to continue looking for new approaches, methods, techniques, including the discovery of mathematical tools that have not been explored yet. Compact magnets for MRI is another source of motivation for finding ultra short gradient coils.

REFERENCES

1. Mansfield P, Grannell PK. 1973. NMR difraction in solids. J Phys C: Solid State Phys 6:L422–L427.
2. Lauterbur PC. 1973. Image formation by induced local interactions: examples employing nuclear magnetic resonance. Nature 242:190–191.
3. Jackson JD. 1998. Classical Electrodynamics. Wiley: New York.

4. Turner R. 1988. Minimum inductance coils. Phys E Sci Instrum 21:948–952.

5. Turner R. 1993. Gradient coil design: a review of methods. Magn Reson Imaging 11:903–920.

6. Turner R, Bowley RM. 1986. Passive screening of switched magnetic field gradients. J Phys E: Sci Instrum 19:876–879.

7. Schmitt F, Irnich W, Fischer H. 1998. Physiological Side Effects of Fast Gradient Switching in Echo Planar Imaging. Springer-Verlag: Berlin, Chapter 3.

8. Turner R. 1986. A target field approach to optimal coil design. J Phys D: Appl Phys 19:L147–L151.

9. Carlson JW, Derby KA, Hawryszko KC, Weideman M. 1992. Design and evaluation of shielded gradient coils. Magn Reson Med 26:191–206.

10. Xu H, Conolly SM, Scott GC, Macovski A. 1999. Fundamental scaling relations for homogeneous magnets. In: Proceedings of the ISMRM 7th Scientific Meeting, Philadelphia, PA, p 475.

11. Silva AC, Merkle H. 2003. Hardware considerations for functional magnetic resonance imaging. Concepts Magn Reson A 16:35–49.

12. Sabate J, Garces LJ, Szczesny PM, Qiming L, Wirth WF. 2004. High-power high-fidelity switching amplifier driving gradient coils for MRI systems. In: Proceedings of the 35th Annual IEEE Power Electronics Specialists Conference, Germany.

13. While PT, Forbes LK, Crozier S. 2010. Designing gradient coils with reduced hot spot temperatures. J Magn Reson 203:91–99.

14. Poole M, Weiss P, Sanchez-Lopez H, Ng M, Crozier S. 2010. Minimax current density coil design. J Phys D: Appl Phys 43:095001.

15. Lopez HS, Liu F, Poole M, Crozier S. 2009. Equivalent magnetization current method applied to the design of gradient coils for magnetic resonance imaging. IEEE Trans Magn 45:767–775.

16. Andrew ER, Szcesniak E. 1995. Low inductance transverse gradient system of restricted length. Magn Reson Med 13:607–613.

17. Mansfield P, Chapman BLW, Bowtell R, Glover P, Coxon R, Harvey PR. 1995. Active acoustic screening: reduction of noise in gradient coils by Lorentz force balancing. Magn Reson Med 33:276–281.

18. Wang F, Mechefske C. 2008. Vibration analysis and testing of a thin-walled gradient coil model. J Sound Vib 311:554–566.

19. Wang F, Mechefske C. 2007. Dynamic analysis of a multi-layered gradient coil insert in a 4T MRI scanner. Concepts in Magn Reson B 31:237–254.

20. Demas V, Prado PJ. 2009. Compact magnets for magnetic resonance. Concepts Magn Reson A 34:48–59.

21. Glover P. 2009. Interaction of MRI field gradients with the human body. Phys Med Biol 54:R99–R115.

22. Schenck JF, Edelstein WA, Hart HR, Williams CS, Bean CP, Bottomley PA, et al. 1983. Switched gradients and rapidly changing magnetic-field hazards in NMR imaging. Med Phys 10:133–133.

23. Hidalgo-Tobon SS, Bencsik M, Bowtell R. 2004. Reduction of peripheral nerve stimulation via the use of combined gradient and uniform field coils. In: ISMRM, Kyoto, Japan; Abstract No. 659.

24. Hidalgo-Tobon SS. 2005. Novel Gradient Coils. PhD Thesis, The University of Nottingham.

25. International Commission on Non-Ionizing Radiation Protection. 1998. ICNIRP Guidelines for Limiting Exposure to Time-Varying Electric, Magnetic, and Electromagnetic Fields International Commission on Non-Ionizing Radiation Protection. Health Physics 74:494–522.

26. Harvey PR, Katznelson E. 1999. Modular gradient coil: a new concept in high-performance whole-body gradient coil design. Magn Reson Med 42:561–570.

27. Kimmlingen R, Gebhardt M, Schuster J, Brand M, Schmitt F, Haase A. 2002. Gradient system providing continuously variable field characteristics. J Magn Reson Med 47:800–808.

28. Chronik B, Rutt B. 2001. A simple linear formulation for magnetostimulation specific to MRI gradient coils. Magn Reson Med 45:916–919.

29. Zhang B, Yen Y, Chronik B, McKinnon G, Schaefer D, Rutt B. 2003. Peripheral nerve stimulation properties of head and body gradient of various sizes. Magn Reson Med 50:50–58.

30. Faber S, Hoffmann A, Ruedig Ch, Reiser M. 2003. MRI-induced stimulation of peripheral nerves: dependency of stimulation threshold on patient positioning. Magn Reson Imaging 21:715–724.

31. Bencsik M, Bowtell R, Bowley R. 2007. Electric fields induced in the human body by time-varying magnetic field gradients in MRI: numerical calculations and correlation análisis. Phys Med Biol 52:2337–2353.

32. Schaefer D, Bourland J, Nyenhuis J. 2000. Review of patient safety in time-varying gradient fields. J Magn Reson Imaging 12:20–29.

33. Roméo F, Hould DI. 1984. Magnet field profiling: analysis and correcting coil design. Magn Reson Med 1:44–65.

34. Golay MJE. Magnetic Field Control Apparatus. US Patent 3,515,979. November 4, 1957.

35. Purcell EM. 1989. Helmholtz coils revisited. Am J Phys 57:18–22.

36. Frenkiel TA, Jasinski A, Morris PG. 1988. Apparatus for generation of magnetic field gradient waveforms for NMR imaging. J Phys E: Sci Instrum 21:374–377.

37. Suits BH, Wilken DE. 1989. Improving magnetic field gradient coils for NMR imaging. J Phys E: Sci Instrum 22:565–573.

38. Siebold H. 1990. Gradient field coils for MR imaging with high spectral purity. IEEE Trans Magn 26:897–900.

39. Vegh V, Zhao H, Brereton IM, Galloway GJ, Doddrell DM. 2006. A wave equation technique for designing compact gradient coils. Concepts Magn Reson B 29:62–64.

40. Lu H, Jesmanowicz A, Li Sh, Hyde J. 2004. Momentum-weighted conjugate gradient descent algorithm for gradient coil optimization. Magn Reson Med 51:158–164.

41. Crozier S, Doddrell D. 1993. Gradient-coil design by simulated annealing. J Magn Reson Ser A 103:354–357.

42. Crozier S, Forbes LK, Doddrell DM. 1994. The design of transverse gradient coils of restricted length by simulated annealing. J Magn Reson Ser A 107:126–128.

43. Peters A, Bowtell R. 1994. Biplanar gradient coil design by simulated annealing. MAGMA 2:387–389.

44. Hoult DI. 1973. The application of high field nuclear magnetic resonance. PhD Thesis, Oxford University.

45. Compton RC. 1982. Gradient coil apparatus for a magnetic resonance system. US Patent 4,456,881.

46. Schweikert KH, Krieg R, Noack F. 1988. A high-field air-cored magnet coil design for fast-field-cycling NMR. J Magn Reson 78:77–96.

47. Wong EC, Jesmanowicz A, Hyde JS. 1991. Coil optimization for MRI by conjugate gradient descent. Magn Reson Med 21:39–48.

48. Chronik B, Rutt B. 1998. Constrained length minimum inductance gradient coil design. Magn Reson Med 39:270–278.

49. Abramowitz M, Stegun IA. 1965. Handbook of Mathematical Functions. Dover, New York.

50. Mansfield P, Chapman B, Turner R, Roger M.1990. Magnetic Field Screens. US Patent 4,978,920.

51. Vavrek R, Schaefer D, Myers Ch, McFarland T, Turner R. 1993. Local Gradient Coil. US Patent 5,185,576.

52. Hidalgo S, Gadzinski C, Rutt B. 2009. Comparison between CCMI and CAHM for design shielded gradient coils for MRI. In: Proceedings of the ISMRM, Honolulu, HI; Abstract No 3057.

53. Lemdiasov A, Reinhold L. 2005. A stream function method for gradient coil design. Concepts Magn Reson B Mag Reson Eng 26:67–80.

54. Poole M, Bowtell R. 2007. Novel gradient coils designed using a boundary element method. Concepts Magn Reson B 31:162–175.

55. Poole M, Sanchez Lopez, Crozier S. 2009. Adaptively regularised gradient coils for reduced local heating. Concepts Magn Reson B 33:220–227.

56. Poole M. 2007. Improved Equipment and Techniques for Dynamic Shimming in High Field MRI. PhD Thesis, The University of Nottingham.

57. Pissanetzky S. 1992. Minimum energy MRI gradient coils of general geometry. Meas Sci Technol 3:667–673.

58. Peeren GN. 2003. Stream function approach for determining optimal surface currents. J Comput Phys 191:305–321.

59. Poole M, Bowtell R, Green D, Pittard S, Lucas A, Hawkes R, Carpenter A. 2009. Split gradient coils for simultaneous PET-MRI. Magn Reson Med 62:1106–1111.

60. Shou G, Xia L, Liu F, Zhu M, Li Y, Crozier S. 2010. MRI coil design using boundary-element method with regularization technique: a numerical calculation study. IEEE Trans Magn 46:1052–1059.

61. Krawczyk-Stando D, Rudnicki M. 2007, Regularization parameter selection in discrete ill-posed problems—the use of U-Curve. Int J Appl Math Comput Sci 17:157–164.

62. Tikhonov AN. 1963. Solution of incorrectly formulated problem and the regularization method. Soviet Math Dokl 4:1035–1038.

63. Tikhonov AN. 1963. Regularization of incorrectly posed problems. Soviet Math Dokl 4:1624–1627.

64. Bowtell R, Bencsik M, Bowley R. 2003. Reducing peripheral nerve stimulation due to switched transverse field gradients using an additional concomitant field coil. In: International Society for Magnetic Resonance in Medicine International Meeting, Toronto, Canada; Abstract No 2424.

65. Sánchez H, Liu F, Trakic A, Crozier S. 2007. A simple relationship for high efficiency–gradient uniformity tradeoff in multilayer asymmetric gradient coils for magnetic resonance imaging. IEEE Trans Magn 43:523–533.

66. Liu Q, Mantone A, McKinnon G, Sellers M. 2007. An efficient multiple field of view gradient coil set. Proc Int Soc Magn Reson Med 15:994.

67. Goodrich KC, Hadley JR, Moon S, Chronik BA, Scholl TJ, Debever JT, et al. 2009. Design, fabrication, and testing of an insertable double-imaging-region gradient coil. Concepts Magn Reson B 35:98–105.

68. Labros S. Petropoulos M, Morich A. 1995. Novel gradient coil set with canceled net thrust force for nuclear magnetic resonance applications. IEEE Trans Magn 31:3536–3539.

69. Alsop D, Connick T. 1996. Optimization of torque-balanced asvmmetric head j gradient coils. Magn Reson Med 35:875–888.

70. Liu H, Petropoulos L. 1997. Spherical gradient coil for ultrafast imaging. J Appl Phys 81:3853–3855.

71. Liu H, Petropoulos LS. 1997. Spherical gradient coil for ultrafast imaging. J Appl Phys 81:3853–3856.

72. Green D, Legget J, Bowtell R. 2005. Hemispherical gradient coils for magnetic resonance imaging. Magn Reson Med 54:656–668.

73. Mansfield P, Chapman BJ. 1986. Active magnetic screening coils in NMR imaging. Magn Reson 66:573–576.

74. Mansfield P, Chapman BJ. 1986. Active magnetic screening of coils for static and time-dependent magnetic field generation in NMR imaging. Phys E: Sci Instrum 19:541–546.

75. Mansfield P, Chapman B. 1987. Multishield active magnetic screening of coil structures in NMR. J Magn Reson 72:211–223.

76. Roemer PB, Hickey. 1986. Self-shielded gradient coils for unclear magnetic resonance imaging. European Patent Application 87,101,198.

77. Bowtell R, Mansfield P. 1991. Gradient coil design using active magnetic screening. Magn Reson Med 17:15–21.

78. Chapman BLW, Mansfield P. 1995. Quiet gradient coils—active acoustically and magnetically screened distributed transverse gradient designs. Meas Sci Technol 6:349–354.

79. Crozier S, Doddrell DM. 1995. A design methodology for short, whole-body, shielded gradient coils for MRI. Magn Reson Imaging 13:615–620.

80. Forbes L, Crozier S. 2004. Novel target-field method for designing shielded bi-planar shim and gradient coils. IEEE Trans Magn 40:1929–1938.

81. Leggett J, Crozier S, Bowtell R. 2003. Actively shielded multi-layer gradient coil designs with improved cooling properties. J Magn Reson 165:196–207.

82. Brown R, Shvartsman S. 1999. Supershielding: confinement of magnetic fields. Phys Rev Lett 83:1946–1949.

83. Shvartsman Sh, Morich M, Demeester G, Zhai Z. 2005. Ultrashort shielded gradient coil design with 3D geometry. Concepts Magn Reson B 26:1–15.

84. Martens MA, Petropoulos LS, Brown RW, Andrews JH, Morich MA, Patrick JL. 1991. Insertable biplanar gradient coil for MR imaging. Rev Sci Instrum 62:2639–2645.

85. Van Vaals JJ, Bergman AH. 1990. New high frequency resonator for NMR imaging and spectroscopy. J Magn Reson 89:331–342.

86. Mansfield P, Morris PG. NMR Imaging in Biomedicine. Academic Press: New York, 1982.

87. Martens MA, Petropoulos LS, Brown RW, Andrews JH, Morich MA, Patrick JL. 1991. Insertable biplanar gradient coils for magnetic resonance imaging. Rev Sci Instrum 62:2639–2645.

88. Bowtell R, Robyr P. 1998. Multilayer gradient coil design. J Magn Reson 131:286–294.

89. Tomasi D, Caparelli EC, Panepucci H, Foerster B. 1999. Fast optimization of a biplanar gradient coil set. J Magn Reson 140:325–339.

90. Moon CH, Park HW, Lee WY. 1999. A design method of minimum-inductance planar MRI gradient coils considering pole piece effect. J Sci Technol 10:136–141.

91. Dodd SJ, Ho C. 2002. Short planar gradient coils for MR microscopy using concentric return paths. J Magn Reson 156:1–9.

92. Lemdiasov R, Ludwig R, Brevard ME, Ferris CF. 2004. Design and implementation of a uniplanar gradient field coil for magnetic resonance imaging. J Magn Reson Eng B 20:17–29.

93. Vegh V, Zhao H, Doddrell DM, Brereton IM, Galloway GJ. 2005. The design of planar gradient coils. Part II: a weighted superposition method. Concepts Magn Reson B 27:25–33.

94. Vegh V, Zhao H, Galloway GJ, Doddrell DM, Brereton IM. 2005. The design of planar gradient coils. Part I: a winding path correction method. Concepts Magn Reson B 27:17–24.

95. Bowtell R, Mansfield P. 1989. Minimum power, flat gradient pairs for NMR microsopy. Proceedings of the 8th Annual Meeting International Society of Magnetic Resonance Imaging. Amsterdam, p 977.

96. Tomasi D. 2006. Optimization of biplanar gradient coils for magnetic resonance imaging. Braz J Phys 36:23–27.

97. Forbes LK, Brideson MA, Crozier SA. 2005. Target-field method to design circular biplanar coils for asymmetric shim and gradient fields. IEEE Trans Magn 41:2134–2144.

98. Liu W, Zu D, Tang X, Guo H. 2007. Target-field method for MRI biplanar gradient coil design. J Phys D 40:4418–4424.

99. Liu W, Zu D. 2007. Research on target-field method for designing gradient coil in permanent-magnet MRI system. In: Progress in Electromagnetics Research Symposium, Beijing, China, pp 1894–1897.

100. Liu H. 2000. An efficient geometric image distortion correction method for a biplanar planar gradient coil. Magn Reson Mater Phys Biol Med 10:75–79.

101. Plewes DB, Silver S, Starkoski P, Walker C. 2000. Magnetic resonance imaging of ultrasound fields: gradient characteristics J Magn Reson Imaging 11: 452–457.

102. Pichler BJ, Wehrl HF, Kolb A, Judenhofer MS. 2008. PET/MRI: the next generation of multi-modality imaging? Semin Nucl Med 38:199–208.

103. Pichler B, Judenhofer M, Catana C, Walton J, Kneilling M, Nutt R, et al. 2006. Performance test of an LSO-APD detector in a 7-T MRI scanner for simultaneous PET/MRI. J Nucl Med 47:639–647.

104. Poole M, Bowtell R, Green D, Pittard S, Lucas A, Hawkes R, et al. 2009. Split gradient coils for simultaneous PET-MRI. Magn Reson Med 62:1106–1111.

105. Andrew ER, Kempka M. 1998. Transverse gradient coil with circle current paths. Magn Reson Mater Phys Biol Med 7:55–60.

106. While PT, Forbes LK, Crozier S. 2009. 3D gradient coil design—initial theoretical framework. IEEE Trans Biomed Eng 56:1169–1183.

107. Moon H, Park H, Cho M, Lee Y. 2000. Design of convex-surface gradient coils for a vertical-field open MRI system. Meas Sci Technol 11:N89–N94.

108. Tomasi D. 2001. Stream function optimization for gradient coil design. Magn Reson Med 45:505–512.

109. Ruset I, Tsai L, Mair R, Patz S, Hrovat M, Rosen M, et al. 2006. A system for open-access 3He human lung imaging at very low field. Concepts Magn Reson B 29:210–221.

110. Leggett J, Crozier S, Blackband S, Beck B, Bowtell RW. 2003. Multilayer transverse gradient coil design. Concepts Magn Reson B 16:38–46.

111. Crozier S, Doddrell DMA. 1998. Simple design methodology for elliptical cross-section, transverse, asymmetric, head gradient coils for MRI. IEEE Trans Biomed Eng 45:945–948.

112. Forbes LK, Brideson MA, Crozier S, While PT. 2007. An analytical approach to the design of quiet cylindrical asymmetric gradient coils in MRI. Concepts Magn Reson B 31:218–236.

113. Zhang B, Gazdzinski C, Chronik BA, Xu H, Conolly S, Rutt B. 2005. Simple design guidelines for short MRI systems. Concepts Magn Reson B Magn Reson Eng 25:53–59.

114. While P, Forbes L, Crozier S. 2009. 3D gradient coil design—toroidal surfaces. J Magn Reson 198: 31–40.

BIOGRAPHY
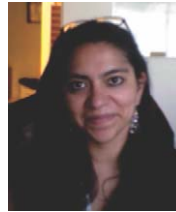
Silvia Hidalgo studied physics (B.Sc. 1998) at the Universidad de las Americas Puebla, and continued with graduate studies (M.Sc. 2000) at the Universidad Nacional Autonoma de Mexico, her Ph.D. degree in physics (magnetic resonance imaging) in 2006 from the University of Nottingham, Britain, and a postdoctoral position at Robarts Research Institute (2006–2008). She is currently working at the Department of Electrical Engineering of the University Autonoma Metropolitana-Iztapalapa. Her scientific interests include development and electromagnetic simulation of RF and gradient coils for MRI applications and molecular imaging by MRI.